Journal of Materials Chemistry C

PAPER

View Article Online
View Journal | View Issue

Cite this: J. Mater. Chem. C, 2016, 4, 7026

Ultraviolet and blue cathodoluminescence from cubic Y_2O_3 and Y_2O_3:Eu^{3+} generated in a transmission electron microscope

D. den Engelsen,[a] G. R. Fern,[a] T. G. Ireland,*[a] P. G. Harris,[a] P. R. Hobson,[b] A. Lipman,[a] R. Dhillon,[a] P. J. Marsh[a] and J. Silver[a]

Received 29th April 2016,
Accepted 5th July 2016

DOI: 10.1039/c6tc01750a

www.rsc.org/MaterialsC

Herein we describe the investigation of cubic spherical submicron particles of non-doped Y_2O_3 and Y_2O_3 doped with Eu^{3+} in a transmission electron microscope (TEM) equipped with a spectrometer to detect cathodoluminescence from individual particles. Each submicron particle was made up of nanometre sized crystals. We found that these crystals showed a broad emission band at 353 nm upon bombardment with 200 keV or 80 keV electrons. Upon increasing the Eu^{3+} concentration from 0 to 2 mol% this UV/blue emission was gradually quenched: at Eu^{3+} concentrations >2 mol% no UV/blue emission was detected, only the well-known cathodoluminescence (CL) spectrum of Y_2O_3:Eu^{3+} could be recorded. This UV/blue emission has been attributed to the intrinsic luminescence of Y_2O_3 caused by self-trapped excitons. We found that the UV/blue luminescence was strongly temperature dependent and that the trap depth of the self-trapped excitons was 0.14 eV. The ratios of the spectral radiances of $^5D_1 \rightarrow {}^7F_J$ and $^5D_0 \rightarrow {}^7F_J$ (J = 0, 1…6) Eu^{3+} transitions in the CL-TEM spectra of Y_2O_3:Eu^{3+} at low Eu^{3+} concentrations was about a factor of 10 larger than those recorded at 15 keV. This phenomenon has been explained by absorption of the intrinsic luminescence of Y_2O_3 by Eu^{3+}.

1. Introduction

Yttrium oxide (Y_2O_3:Eu^{3+}) is a well-known phosphor from its application as the red emitting phosphor in fluorescent lamps and projection cathode ray tubes (CRTs).[1–3] Due to the industrial applications and the attractive properties of Y_2O_3 as host lattice, Y_2O_3 doped with Eu^{3+} and other rare earth ions has been well studied and documented. The expected application of Y_2O_3:Eu^{3+} in low-voltage field emission displays has stimulated intensive research in the synthesis and characterisation of nanosized phosphors, recently reviewed by Li and Lin.[4] In our laboratory we have studied the enhancement of cathodoluminescence by applying double layers of ZnO:Zn and Y_2O_3:Eu^{3+}.[5] Non-doped Y_2O_3 also yields photoluminescence when excited with UV radiation. Although this has been known for more than 50 years,[6] the luminescence of non-doped Y_2O_3 has not been studied in much detail until recently. The reason for this recent interest is the possible application of non-doped Y_2O_3 and Y_2O_3 doped with Eu^{3+}, Tb^{3+}, Nd^{3+} or Tm^{3+} as a scintillation material.[7–15] When non-doped Y_2O_3 is excited by α-particles,[7] UV-radiation (207 nm)[8] or X-rays,[9–13] a broad luminescence band is observed between 340 nm and 500 nm. Table 1 summarizes the wavelength at maximum (λ_{max}) of this broad luminescence band recorded in the literature. The values for λ_{max} listed in Table 1 vary substantially. This erratic behaviour of the luminescence of Y_2O_3 elicited the following statement from Fukabori *et al.*[7] "Light yields of Y_2O_3 ceramics are different from specimen to specimen. Nature of this phenomenon is not clear yet". Konrad *et al.*[8] found that the size of nanoparticles plays an important role and might explain a variation of about 30 nm in λ_{max}; however, this does not explain the variation shown in Table 1. Fukabori *et al.*[7] found a relation between the scintillation light output and crystal size in their Y_2O_3 samples: the larger the crystallites, the higher the light output.

Table 1 λ_{max} of luminescence band of non-doped cubic Y_2O_3

λ_{max} (nm)	Type of excitation	Ref.
410	UV: 248 nm	6
340	UV: 207 nm	8
344	UV: 207 nm	12
350	α-particles	7
410	X-ray	9
364	X-ray	10
500	X-ray	11
385	X-ray	13

[a] Centre for Phosphor and Display Materials, Wolfson Centre for Materials Processing, Brunel University London, Uxbridge, Middlesex, UB8 3PH, UK. E-mail: Terry.ireland@brunel.ac.uk
[b] Department of Electronic and Computer Engineering, Brunel University London, Uxbridge, Middlesex, UB8 3PH, UK

Wood and Hayes[10] reported that the 364 nm emission band is particularly strong upon X-ray excitation at 1.6 K; Tanner *et al.*[12] also found that the 344 nm band in Y_2O_3:Eu^{3+} with either 0.1 mol% or 1 mol% Eu^{3+} is strongly temperature dependent.

Besides the position of λ_{max} there is another interesting characteristic of the intrinsic luminescence of Y_2O_3: the quenching of this luminescence upon doping with rare earth ions. This was first noticed by Wickersheim and Lefever[6] and later by Jacobsohn *et al.*[9] and Tanner *et al.*[12] Jacobson *et al.* observed a strong reduction of the intrinsic Y_2O_3 luminescence upon doping with 20 ppm Tb^{3+}, while the intrinsic Y_2O_3 luminescence virtually disappeared at doping with 0.08 at% Tb^{3+}. Hayes *et al.* mention the weak intrinsic luminescence of Y_2O_3 upon doping with Eu^{3+}.[14] This phenomenon has been observed by other workers as well in studies of Y_2O_3 doped with other rare earth ions, although without comment.[15,16] Fukabori *et al.*[15] measured a weak intrinsic band at 350 nm upon doping Y_2O_3 with 1 mol% Nd, while Fujimoto *et al.*[16] measured a weak emission band at 360 nm upon doping with 0.15 mol% Tm^{3+}. These latter authors assigned this band to the emission of Tm^{3+}; however, we believe that the measured emission band is too broad for an emission line of Tm^{3+}. Upon exciting Y_2O_3:Eu^{3+} (5 mol% Eu^{3+}) and Y_2O_3:Tb^{3+} (0.5 mol% Tb^{3+}) with α-particles, Cress *et al.*[17] could not detect any broad emission band in the near UV-blue. This indicates that at these rare earth concentrations the intrinsic Y_2O_3 emission has been quenched completely. Comparing this result with the observation of Hayes *et al.*,[14] it may be concluded that Tb^{3+} is more effectively quenching the intrinsic Y_2O_3 luminescence than Eu^{3+}. Ato *et al.*[18] reported a strong thermo-luminescence peak of Y_2O_3:Eu^{3+} upon irradiation with γ-rays from a Co^{60} source at low and high dose rates. They did not suggest at that time that Eu^{3+} was being reduced by γ-rays: this mechanism was suggested nine years later by Ozawa,[19] a co-author of Ato.[18]

The intrinsic luminescence of Y_2O_3 has been explained by three different mechanisms: (1) oxygen vacancies,[9] (2) self-trapped excitons (STE)[7,8,10,12,14,20,21] and (3) ligand-to-metal charge-transfer involving the empty 3d orbitals of the Y^{3+} ion.[13] The latter two mechanisms are more plausible, because luminescence due to STEs[14] or charge-transfer generates broad bands, while Hayes *et al.*[14] also concluded that the STE-mechanism is likely from their measurements of optical detection of magnetic resonance (ODMR). No explanation is apparent in the literature for the quenching of the intrinsic luminescence of Y_2O_3 upon doping with rare earth ions.

The current density in a projection CRT at normal operating conditions has a maximum at about 0.25 A m^{-2}. There have been no reports of finding blue CL from Y_2O_3:Eu^{3+} in such CRTs. In a scanning electron microscope the beam current at the specimen is normally between 0.01 nA and 1 nA, dependent on the settings of the condenser lenses,[22] and the spot size is often of the order of 1.5 nm, leading to current densities between 6×10^6 A cm^{-2} and 6×10^8 A cm^{-2}, which are 7 to 9 orders of magnitude larger than in a CRT. If the electron transmission at 200 keV is about 99.99% in 200 nm crystals of Y_2O_3, then the effective current density is still 3 to 5 orders of magnitude higher. This difference in effective current density could explain why blue emission was never observed before or previously reported. Another reason is the quenching of this emission at Eu^{3+} concentrations greater than 2 mol% (which is typical for CRTs and fluorescent lamps red phosphors). In our laboratories we are currently involved in cathodoluminescence (CL) and photoluminescence (PL) studies of nanosized and submicron Y_2O_3 doped with Eu^{3+},Tb^{3+} and other rare earth ions.[23–26] Yttrium oxide is a stable compound and when doped with Eu^{3+}, nobody (to our knowledge) has observed broad emission bands between 350 and 500 nm as mentioned above. It was therefore a surprise when investigating Y_2O_3:Eu^{3+} samples in our transmission electron microscope (TEM) equipped with an optical spectrometer that we observed a broad emission band at 350 nm. Preliminary results of this observation have been presented at the 22nd International Display Workshops in Japan.[27] Herein we describe further measurements and present an analysis of the intrinsic emission of non-doped Y_2O_3 and Y_2O_3:Eu^{3+} in the electron beam of a TEM.

2. Materials and methods

Materials and synthesis

Yttrium oxide (99.99%, Ampere Industrie, France) and europium(III) oxide (99.99%, Neo Performance Materials, UK) were used to prepare the europium-doped yttrium nitrate stock solutions. Urea, nitric acid, oxalic acid and isopropanol (IPA) were supplied by (Fisher Scientific, UK). All chemicals were used as received.

The synthesis of sub-micrometre spherical Y_2O_3:Eu^{3+} precursor particles *via* a homogeneous precipitation route utilising the hydrothermal decomposition of urea method, followed by annealing the precursor particles at 980 °C resulting in cubic Y_2O_3:Eu^{3+} has been described extensively in our earlier work.[23–26] The concentration of Eu^{3+} in Y_2O_3 was adjusted to 0.1, 0.5, 1, 1.5, 4, 20, 60 and 100 mol%. For comparison reasons three samples of micrometre sized Y_2O_3:Eu^{3+} precursor particles were prepared *via* an oxalate precipitation route.[1,3] The first sample was made by co-precipitation of Eu^{3+}-oxalate (2%) and Y^{3+}-oxalate. The second and third samples were made by separately precipitating Y^{3+}-oxalate and Eu^{3+}-oxalate (6% and 2%) and then slurry-mixing (SM) these precipitates before annealing. These samples were then annealed for four hours at 980 °C in air.

Transmission electron microscope

The submicron spherical Y_2O_3 and Y_2O_3:Eu^{3+} samples were investigated with a TEM (2100F, JEOL, Japan) equipped with a Schottky-type field emission gun. When operated in scanning mode (STEM), the spot size of the e-beam at the specimen was adjusted to 0.2 nm or 1.5 nm. Initial work demonstrated the need to reduce the X-rays in the column generated from the condenser lens aperture, which were found to significantly contribute to disperse excitation of phosphor samples. These X-rays excited the phosphor and caused the emission of visible

light when the electron beam was not on the sample, leading to unwanted interference and a loss of resolution. To reduce this X-ray excitation of the sample, a hard X-ray aperture was inserted into the column, which reduced the background noise in CL imaging and spectroscopy modes considerably. The TEM was equipped with a Vulcan™ CL detector, Gatan, USA, for imaging and spectroscopic purposes. This system used a Czerny–Turner spectrometer with back-illuminated CCD and a grating with 1200 lines per mm (blazed at 500 nm) for collection of CL emission spectra. Light was collected from the sample using a mirror above and below the sample, which enabled a solid angle of about 5 sr, which is almost half of a sphere. This high solid angle made light collection highly efficient and enabled the collection of CL at low intensity. Unfortunately, the cooled detector of this spectrometer did not allow the recording of spectra at $\lambda < 380$ nm. In the subsequent sections spectra recorded with this spectrometer will be represented at $\lambda > 400$ nm. Spectra between 200 and 400 nm were recorded with the Black Comet spectrometer of StellarNet Inc. (USA) for undoped Y_2O_3. This spectrometer had an uncooled detector and the spectra were therefore much noisier.

By collecting the visible light with the Vulcan system simultaneously with JEOL's high-angle annular dark-field (HAADF) detector, it was possible to observe the visible light that was emitted from the particles. A small cryostat connected to the sample holder enabled cooling of the samples in the TEM down to 102 K (−171 °C); adjustment of the sample temperature anywhere between 102 K and 303 K could be made. A Gatan electron energy loss spectrometer (EELS) was used to map the position of europium ions at the surface of the nanocrystals.

X-ray powder diffraction

The crystalline phases of the products were determined by X-ray powder diffraction (XRPD) using a Bruker D8 Advance X-ray powder diffractometer fitted with a nickel-filtered copper source and a LynxEye™ silicon strip detector. Data were recorded from 5 to 100 2θ degrees at 25 °C. The diffractometer was previously calibrated using an aluminium oxide line position standard from Bruker and a LaB_6 NIST SRM 660a line profile standard. Diffractograms were collected using the annealed powders in a conventional holder. The emission of the nickel filtered Cu source and hence the instrumental line broadening was determined by fitting the NIST standard using Bruker Topas version 3. Phases in the combusted products were identified from the XRD patterns by peak search matching using the ICCD PDF-2 data files.

3. Results

Transmission electron microscope analysis

Fig. 1a is a TEM image of the urea-precipitated cubic spherical submicron Y_2O_3:Eu^{3+} phosphor particles with diameters between 200 nm to 300 nm. Fig. 1b presents a TEM image of a single particle, which is composed of a number of tessellated nanocrystals from 40 nm to 80 nm.

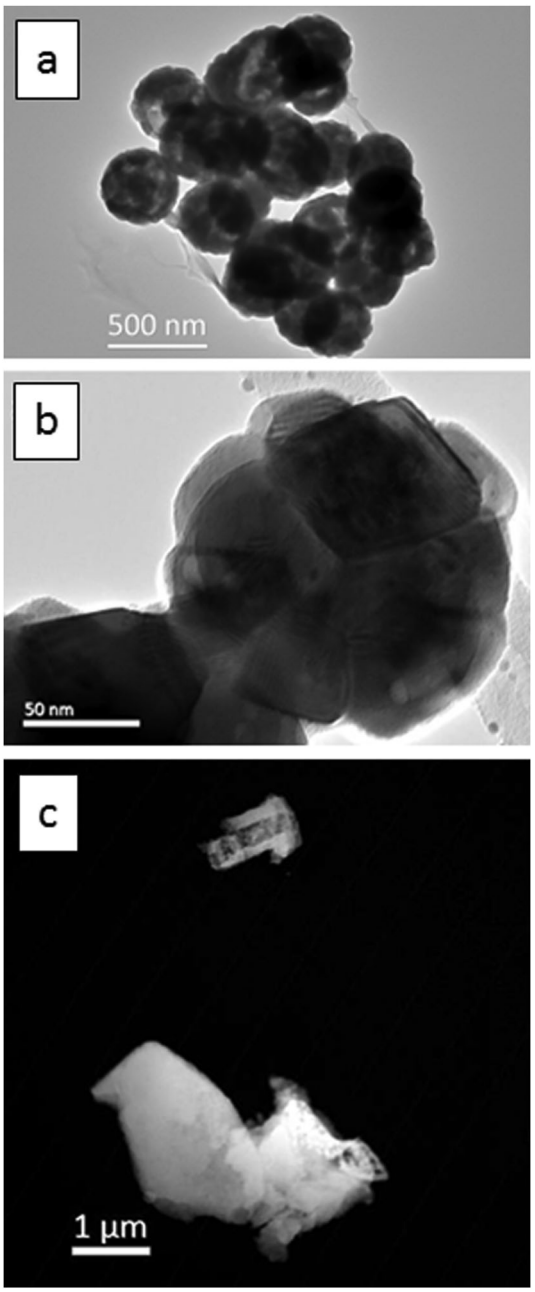

Fig. 1 TEM images, (a) and (b), of Y_2O_3:Eu^{3+} particles: (a) urea-precipitated route, (b) higher magnification image of a single particle from (a). (c) HAADF image oxalate-precipitated particles.

In Fig. 1c the oxalate-precipitated cubic micrometre sized Y_2O_3:Eu^{3+} phosphor particles are presented. These have an irregular morphology with a size range between 1 and 3 micrometres.

X-ray diffraction

X-ray diffraction was only used for the analysis of the oxalate-precipitated samples of Y_2O_3:Eu^{3+}, because urea-precipitated samples of Y_2O_3 and Y_2O_3:Eu^{3+} after annealing at 980 °C for 4 hours are known to consist of the cubic phase for 100%.[23–26] Fig. 2 shows the diffractogram for oxalate-precipitated Y_2O_3:Eu^{3+}.

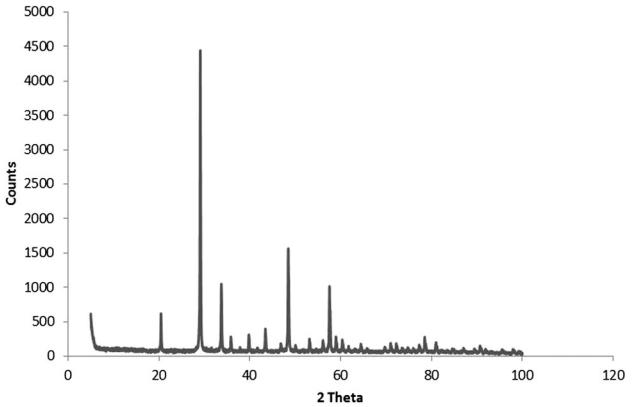

Fig. 2 Powder X-ray diffractogram of Y_2O_3:Eu^{3+} (2%) oxalate method co-precipitated. Fired at 980 °C for 4 hours.

This diagram proved that this material after annealing for 4 hours at 980 °C also consisted for >99% of the cubic phase.

UV/blue emission band

Fig. 3 shows a spectrum of undoped Y_2O_3 excited with an electron beam of 200 keV at −120 °C. The as-recorded spectrum is the noisy curve (1), which is represented by a Gaussian profile (3) corrected for the background (2). The Gaussian profile has been fitted to the spectrum with a least squares algorithm using Microsoft's Excel solver.

By averaging the values for λ_{max} and the full width at half maximum (FWHM) from spectra recorded at various temperatures, we determined that λ_{max} = 353 nm (28 300 cm^{-1}) and FWHM = 5735 cm^{-1}. This value of λ_{max} is identical to the value published by Fukabori *et al.*[7] and close to the values published by Konrad *et al.*,[8] Wood and Hayes[10] and Tanner *et al.*[12] Fukabori *et al.* found that in some of their samples the emission extended much further in the visible region. This has not been confirmed in our measurements, neither in those of the other workers.[8–10,12,13] Nevertheless, the broad UV emission band represented in Fig. 4 extends substantially into the visible part of electromagnetic radiation. At 405 nm the

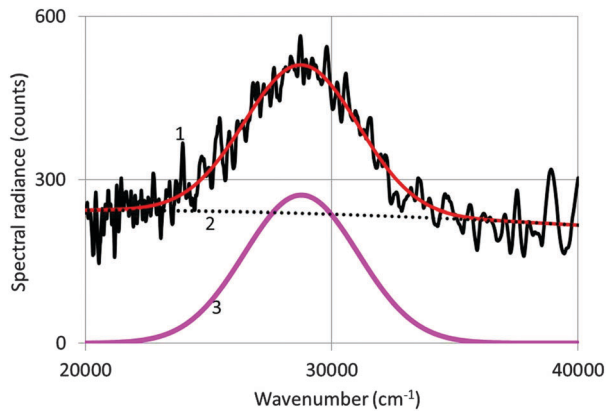

Fig. 3 Spectrum of undoped Y_2O_3 excited with an electron beam of 200 keV and spot size 1.5 nm at −120 °C (1). Recorded with the StellarNet spectrometer with an integration of 16 s. (2): Background. (3): Gaussian profile fitted to the data points and corrected for background.

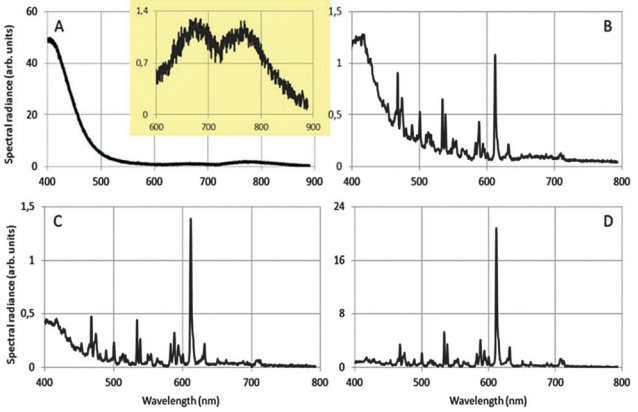

Fig. 4 CL spectra of Y_2O_3:Eu^{3+} recorded at −171 °C, 200 keV beam voltage and spot size of 1.5 nm. (A) non-doped Y_2O_3, inset: spectrum at larger scale between 600 nm and 900 nm; (B) 0.1 mol% Eu^{3+}; (C) 0.5 mol% Eu^{3+}; (D) 1 mol% Eu^{3+}. The sharp lines in the spectrum are Y_2O_3:Eu^{3+} transitions; the strongest is the $^5D_0 \rightarrow {}^7F_2$ Eu^{3+} transition at 611 nm.

spectral radiance is almost 5 times smaller than at 353 nm; however, for comparing the intrinsic Y_2O_3 luminescence with the Eu^{3+} emission lines for the doped samples, we used the Gatan spectrometer with the cutoff at about 390 nm, basically because of the detector limitation of the StellarNet spectrometer.

Fig. 4 shows how we were able to turn the red-emitting phosphor Y_2O_3:Eu^{3+} into a UV/blue-emitting phosphor in the TEM: the radiance of the UV/blue luminescence is dwarfing the (area) radiance of the well-known emission lines of Eu^{3+} in Y_2O_3 at 0.1 mol% Eu^{3+}. Important conditions for observing the broad UV luminescence are: low temperature of the sample: −171 °C, large spot size of the e-beam of 1.5 nm, high beam current by maximising the condenser lens aperture and a specimen thickness of at least 100 nm. The energy of the electron beam does not seem paramount: we observed the UV/blue luminescence both at 200 keV at 80 keV. In Fig. 4A the sharp emission lines of Eu^{3+} are not present: whereas the strongest transition in Fig. 4B–D is that due to the $^5D_0 \rightarrow {}^7F_2$ Eu^{3+} transition at 611 nm. The vertical scales of the graphs in Fig. 4 cannot be compared due to the different integration times during spectra recording and different specimen thicknesses. It can be seen that the spectral radiance (normalised to the spectral radiance at 611 nm) of the blue emission at 400 nm decreases strongly when the concentration of Eu^{3+} is increased from 0.1 to 1 mol%. At Eu^{3+} concentrations ≥2 mol% in urea-precipitated Y_2O_3:Eu^{3+} we could not detect any UV/blue emission at 400 nm. Beside the strong UV/blue emission at 400 nm, two very weak long wavelength bands can be observed (inset of Fig. 4A), one at about 675 nm and the other at about 770 nm. Electron bombardment of the carbon-coated Cu-grid without Y_2O_3:Eu^{3+} particles did not show any CL; hence, interference from the Cu-grid holder material can be excluded.

The luminescence spectrum between 400 nm and 500 nm in Fig. 4A (and the weak long wavelength bands) did not noticeably change its shape upon reducing the energy of the electron beam from 200 keV to 80 keV. This therefore excludes Cherenkov radiation being the origin of the observed emission bands at

353 nm, 675 nm and 770 nm.[28] At 400 nm the refractive index of Y_2O_3 is 1.98: to calculate the refractive index of Y_2O_3 as a function of λ, use was made of the dispersion formula given by Nigara.[29] The condition for Cherenkov radiation in a medium with a refractive index of 1.98 is satisfied when the electron velocity $>1.52 \times 10^8$ m s^{-1}, which starts at an electron energy of 80 keV. So, at 80 keV there cannot be Cherenkov radiation in Y_2O_3 at wavelengths $>\sim$405 nm. From this straightforward calculation it can be concluded that any light at wavelengths $>$405 nm that is emitted upon bombarding non-doped, transparent Y_2O_3 crystals with electrons at 80 keV cannot be ascribed to Cherenkov radiation. Since the position and shape of the blue emission did not change upon increasing the electron energy to 200 keV, we can reasonably exclude Cherenkov radiation for 200 keV electrons as well. Additional evidence for this conclusion is the strong temperature dependence of the UV/blue and red emission, as we shall discuss in the following paragraphs. Cherenkov radiation is virtually not affected by temperature as long as the refractive index and the density of the specimen do not change substantially. In ref. 27 it was supposed that the blue emission of Y_2O_3:Eu^{3+} at 400 nm was caused by reduction of Eu^{3+} to Eu^{2+}. From Fig. 4A it must be concluded that this is not the case and that the blue emission in all graphs of Fig. 4 is intrinsic luminescence of Y_2O_3. In other words, it is concluded that the UV/blue luminescence observed in the TEM is identical to the blue/UV emission from undoped Y_2O_3 and Y_2O_3 doped with small amounts of rare earth ions upon excitation by other sources of ionizing radiation.[7–16]

In order to quantify the quenching of the intrinsic luminescence of Y_2O_3 upon increasing the Eu^{3+} concentration we define a quenching factor η:

$$\eta = \frac{SR_{405}}{SR_{405} + SR_{611}}, \quad (1)$$

where SR_{405} is the spectral radiation of the UV/blue emission at 405 nm and SR_{611} is the spectral radiance of the $^5D_0 \rightarrow {}^7F_2$ Eu^{3+} transition at 611 nm. For non-doped Y_2O_3 η = 1 and for Eu^{3+} concentrations $>$2 mol%, η = 0.

Fig. 4B–D refer to Y_2O_3 doped with 0.1, 0.5 and 1 mol% Eu^{3+}. Apart from the diminishing intrinsic luminescence of the host material there is another interesting phenomenon, *viz.* the changing ratios between the spectral radiance of the strongest Eu^{3+} transition at 611 nm and the spectral radiances of Eu^{3+} transitions at $\lambda <$ 611 nm. Furthermore, these latter transitions are about two orders of magnitude stronger than the corresponding transitions in the photoluminescence (PL) spectrum of Y_2O_3:Eu^{3+} as represented in Ozawa's book on page 165.[3] We shall discuss these phenomena together with the intrinsic luminescence of Y_2O_3 in the next section.

Fig. 5 is a HAADF image of urea-precipitated Y_2O_3:Eu^{3+} (0.1 mol% Eu^{3+}) at −168 °C and 200 keV. The image illustrates the effect of positioning of the e-beam on η. The square denoted by "Spatial Drift" indicates the image that was used to compensate the thermal drift of the sample holder during cooling and warming up. This feature enabled a stable position of the electron beam on the nanocrystal during recording of the spectra, which required more than 2 minutes in some cases. The sites SI.1 to SI.5 in Fig. 5 refer to spots with different particle thickness: SI.1 is a very small particle, whereas SI.2 and SI.3 refer to spots with two particles on top of each other.

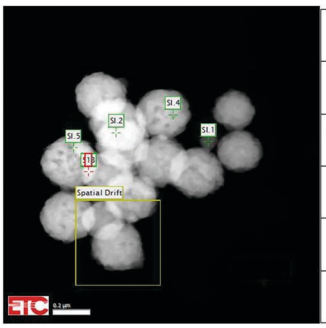

Site	SR_{405}	SR_{612}	η
SI-1	0.5	2.6	0.16
SI-2	12.2	10.8	0.53
SI-3	5.3	10.2	0.34
SI-4	3.3	5.6	0.37
SI-5	2.5	8.4	0.23

Fig. 5 Quenching factor η at various sites for urea-precipitated Y_2O_3:Eu^{3+} (0.1 mol% Eu^{3+}) at −168 °C and 200 keV.

This is reflected in the rather high value for the Eu^{3+} emission. In the other urea-precipitated samples of Y_2O_3:Eu^{3+} containing larger Eu^{3+} concentrations, the variation of the quenching factor η was less than a factor of two. Since some Y_2O_3:Eu^{3+} particles are partially hollow, it is impossible to determine a relation between R_{405} and R_{611} and specimen thickness from Fig. 5. It should be kept in mind that the radiance R_b of the Y_2O_3 emission band, defined as

$$R_b = \int_{b-}^{b+} SR(\lambda)d\lambda \quad (2)$$

where $b-$ and $b+$ are the integration limits, is outstripping the radiance of the $^5D_0 \rightarrow {}^7F_2$ Eu^{3+} transition at 611 nm at low Eu^{3+} concentrations, because the UV emission band is much broader than the 611 nm peak.

Fig. 6 shows the effect of temperature on the spectral radiance of the intrinsic emission of undoped Y_2O_3: the lower the temperature, the stronger the UV/blue luminescence. The drift corrector facility, indicated in Fig. 5, guaranteed that the spectra shown in Fig. 6 were recorded at the same spot. Since the time for recording the spectra (integration time) was also kept constant, the spectra for different temperatures can be compared directly: *i.e.* there is no effect of thickness. The intrinsic blue luminescence in Y_2O_3:Eu^{3+} also increased by more than a factor of 10 upon decreasing the temperature from 31 °C to −171 °C.

The two long wavelength bands shown in the inset of Fig. 6 are much weaker than the UV/blue emission and are also stronger at −172 °C than at 30 °C. It can be seen that the temperature behaviour of the band at 675 nm deviates from that of the other band at 770 nm and the UV/blue band. Upon excitation of Y_2O_3 or Y_2O_3:Eu^{3+} by X-rays or α-particles no emission was observed from these bands by other workers.[7,9–11,13–16] These bands also disappeared when the Eu^{3+} concentration was increased. The origin of these two bands is unknown.

Fig. 7 is an Arrhenius plot of the spectral radiance (SR) measured at 353 nm with the StellarNet spectrometer (data points 1) and SRs measured at 405 nm with the Gatan

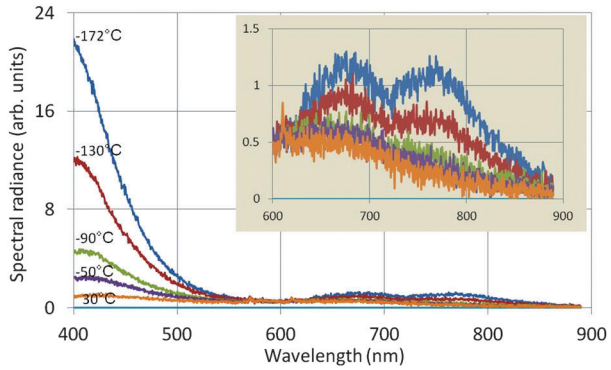

Fig. 6 Spectra of undoped Y_2O_3 recorded at 80 keV and various temperatures. The inset shows the spectra between 600 and 900 nm at a different vertical scale.

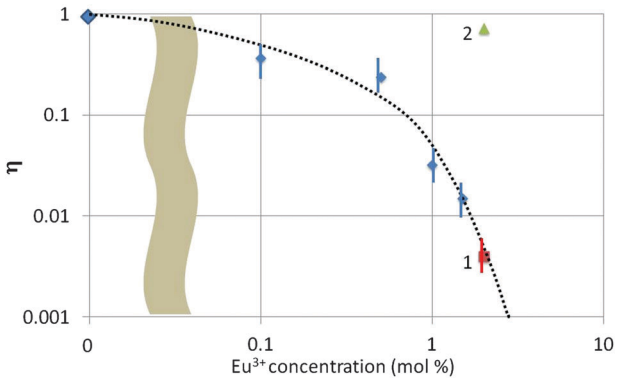

Fig. 8 Quenching factor η as a function of Eu^{3+} concentration in Y_2O_3. (1): oxalate-co-precipitated Y_2O_3:Eu^{3+}, (2) SM-oxalate-precipitated Y_2O_3:Eu^{3+}. Other points refer to urea-precipitated samples. The abscissa is quasi-logarithmic, because the point with 0 mol% Eu^{3+} dope has been indicated.

spectrometer (data points 2 and 3). The data points of (1) refer to undoped Y_2O_3 and 200 keV beam energy, the data points of (2) refer also to undoped Y_2O_3 but at 80 keV and the data points of (3) refer to Y_2O_3:Eu^{3+} with 0.1 mol% Eu^{3+} and 200 keV. The drift corrector facility enabled us to stay at the same point during recording of the spectra and after changing the temperature. In some cases a tiny shift was applied to deal with beam degradation. However, the measured effect of beam degradation on spectral radiance was $<2\%$, which was smaller than the noise level in the spectra, especially in the StellarNet spectra, as shown in Fig. 3. The curves in Fig. 7 have been fitted to the data points with eqn (4) that describes the temperature-dependent effect of STEs. This will be discussed in the next section. The trap depth that describes the experimental data for non-doped Y_2O_3 is 0.13 eV and it is 0.16 eV for Y_2O_3:Eu^{3+} with 0.1 mol% Eu^{3+}. For Y_2O_3:Eu^{3+} with other Eu^{3+} concentrations the Arrhenius plots are similar to that of 0.1 mol% Eu^{3+} as indicated in Fig. 7. In view of the spread in the data we consider that the trap depth of the STEs in undoped and doped Y_2O_3 is identical and has a value of 0.14 eV.

In Fig. 8 we have summarized the quenching factor η (for the blue band) as a function of Eu^{3+} concentration for all samples investigated in the TEM. There are three types of samples collected in Fig. 8, *viz.* urea-precipitated (without a number), oxalate co-precipitated (no. 1) and SM-oxalate precipitated (no. 2). As mentioned above, blue luminescence could not be observed for the urea-precipitated samples at Eu^{3+} concentrations >1.5 mol%, whereas the SM-oxalate samples showed very large blue luminescence for 2 and 6 mol% Eu^{3+}. The spread in η was about a factor of 3 in the SM-oxalate samples; in the urea-precipitated samples it was less.

Fig. 8 illustrates the different behaviour of the SM-oxalate-precipitated and urea-precipitated samples, whereas the oxalate co-precipitated sample (point 1 in Fig. 8) with molecular mixing of the Eu^{3+} and Y^{3+} ions indicates that this sample behaves as the urea-precipitated samples. The deviating behaviour of the SM-oxalate-precipitated sample is explained by its inhomogeneity, in which Eu^{3+}-rich areas in the crystals are alternating with areas with very low Eu^{3+} concentration. The penetration depth of 200 keV electrons in crystalline Y_2O_3 is about 75 μm,[5,30] which is much larger than the size of the oxalate-precipitated crystals. The Eu^{3+} rich areas in the crystal hit by the e-beam do not contribute to the build-up of the blue band because of concentration quenching, whereas the areas with very low Eu^{3+} concentration take care of the strong blue band signal. This hypothesis was confirmed by the very low Eu^{3+} signal in the EELS (not shown) at various spots. From this consideration it can be concluded that the SM-oxalate precipitated sample should be inserted at a much lower concentration in Fig. 8. Since the effective Eu^{3+} concentration is unknown, the best we could do is plotting the result at the as-made Eu^{3+} concentration.

Finally we would like to mention that we also observed blue luminescence in the TEM when bombarding undoped monoclinic Y_2O_3 crystals with 200 keV electrons at 1.5 nm spot size. The monoclinic material was unstable under these electron bombardment conditions, decomposing partly into the more stable cubic form, and therefore we do not reproduce any results of these measurements in this article.

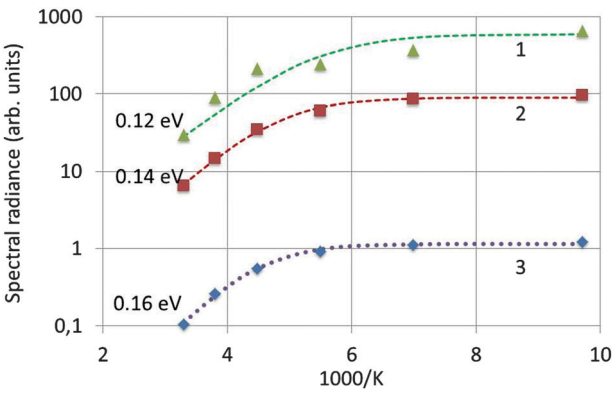

Fig. 7 Arrhenius plot of spectral radiance *versus* 1000 K. (1): SR_{353} of undoped Y_2O_3 recorded at 200 keV; (2): SR_{405} of undoped Y_2O_3 recorded at 80 keV; (3): SR_{405} of Y_2O_3:Eu^{3+} with 0.1 mol% Eu^{3+} recorded at 200 keV. The dashed curves have been fitted to the experimental data with eqn (4).

Discussion of blue luminescence in Y_2O_3 and transition ratios

When an electron beam of 200 keV hits an Y_2O_3 crystal it produces besides defects, backscattered and secondary electrons, X-rays and holes by inelastic scattering processes. Electrons and holes can combine to form free excitons and STEs. Herein we adopt the model that STEs are responsible for the blue luminescence in undoped Y_2O_3 and Y_2O_3:Eu^{3+} as indicated in the literature.[7,8,10,12,14,20,21] According to Mikhailik and Kraus[31] and Blasse[32] the radiance B of a scintillator upon excitation can be written as:

$$B = \alpha N_{e\text{–}h} S Q \quad (3)$$

where α is a proportionality constant, $N_{e\text{–}h}$ is the number of electron–hole pairs that is generated by the electron beam inside the crystal, S is the probability of transferring energy from an e–h pair to a luminescent centre, *e.g.* a Eu^{3+} ion, and Q is the luminescence quantum efficiency. Undoped Y_2O_3 is a so-called self-activated or intrinsic scintillator,[31] in which S is 1 by definition. The intrinsic luminescence in non-doped Y_2O_3 is considered to come from O-2p levels and Y-3d levels after an STE has combined with a luminescent centre in Y_2O_3.[11] The quantum efficiency Q in eqn (3) can be described by Mott's equation on thermal quenching:[31]

$$Q = \frac{P}{1 + C e^{-E_A/kT}} \quad (4)$$

where P and C are constants to be fitted, E_A is the activation or trap energy, k is Boltzmann's constant and T is the absolute temperature. In Fig. 8 we have fitted Q according to eqn (4) to the experimental points for undoped Y_2O_3 and Y_2O_3:Eu^{3+} with 0.1 mol% Eu^{3+}. It can be seen that the experiments are satisfactorily represented with E_A = 0.14 eV both for non-doped Y_2O_3 and 0.1 mol% Y_2O_3:Eu^{3+}. We interpret this activation energy as the trap depth of the self-trapped exciton.

It should be kept in mind that eqn (3) for self-activated Y_2O_3 refers to the radiance of the blue emission band. When Y_2O_3 is doped with Eu^{3+}, energy will be transferred from the host lattice to the Eu^{3+} luminescent centres: hence, the CL spectrum of Y_2O_3:Eu^{3+} can be detected. The CL of Y_2O_3:Eu^{3+} can also be described with an energy transfer probability S in eqn (3), which is 0 for undoped Y_2O_3 and has a maximum value, albeit < 1, for a dopant concentration of 2 mol% and larger.

As mentioned above, Fig. 4 shows that the spectral radiance of Eu^{3+} transitions at $\lambda < 580$ nm decreases in the sequence Fig. 4B–D. We have plotted this behaviour for some transitions in Fig. 9.

Fig. 9 represents the ratios R_1 and R_2, which are the ratios of the spectral radiances $^5D_1 \rightarrow {}^7F_1$ (533 nm) and $^5D_0 \rightarrow {}^7F_2$ (611 nm) and that of $^5D_0 \rightarrow {}^7F_4$ (713 nm) and $^5D_0 \rightarrow {}^7F_2$ (611 nm) respectively. It can be seen that R_1 decreases almost by a factor of 10 upon increasing the dopant concentration from 0.1 mol% to 4%, whereas R_2 is constant, both at cryogenic and room temperature. The latter ratio is constant, because it refers to $^5D_0$ transitions. The transitions of the $^5D_2$ and $^5D_3$ states to the ^7F_J manifold show a similar behaviour as the $^5D_1 \rightarrow {}^7F_1$ transition; however, due to the lower spectral radiances the error bar in the graphs is larger and therefore these will not be reproduced here. The partial concentration quenching of the $^5D_1$ transition of the Eu^{3+} ion represented in Fig. 9 is well known and it has been described by Blasse and Grabmaier[2] and Klaassen *et al.*[33] Blasse and Grabmaier explained the behaviour of R_1 in terms of the following cross relaxation in Eu^{3+}:

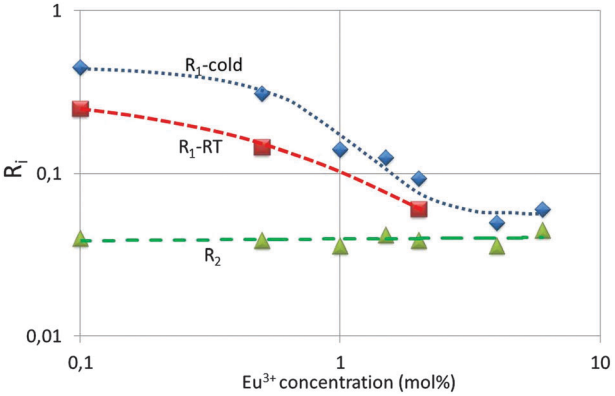

Fig. 9 Ratio of spectral radiance between $^5D_1 \rightarrow {}^7F_1$ (533 nm) and $^5D_0 \rightarrow {}^7F_2$ (611 nm): R_1 and ratio of spectral radiance between $^5D_0 \rightarrow {}^7F_4$ (713 nm) and $^5D_0 \rightarrow {}^7F_2$ (611 nm): R_2. For R_1 the measurements at −170 °C (cold) and room temperature (RT) gave different results.

$$^5D_1 + {}^7F_0 \rightarrow {}^5D_0 + {}^7F_3. \quad (5)$$

This cross relaxation is facilitated by the ten times faster decay rate from $^5D_1$ levels as that from $^5D_0$ levels as indicated by Klaassen *et al.*[33] These latter authors described the partial quenching of ^5D_J (for $J > 0$) transitions in terms of radiative decay time and the rate of non-radiative transfer processes. However, neither cross relaxation nor rate constants explain why R_1 is so large in Fig. 9 at low Eu^{3+} concentrations.

For a qualitative explanation we shall make use of the energy diagram depicted in Fig. 10. Most levels indicated in Fig. 10 have been reported by Wen *et al.*,[34] only the lowest energy level of the manifolds is indicated. The energy level of the intrinsic Y_2O_3 emission band has been centred at 28 300 cm^{-1} above the ground level $^7F_0$ of Eu^{3+}, based on the spectrum depicted in Fig. 4. The level of the STE Y_2O_3 emission band overlaps with several Eu^{3+} levels; hence, it seems obvious that energy can radiationless be transferred from an STE in Y_2O_3 to the $^5D_4$ level of Eu^{3+}, which is only slightly lower. This process, which takes place at Eu^{3+} concentrations >2 mol%, is indicated by arrow 4. From the $^5D_4$ level energy will radiationless trickle down to the $^5D_3$, $^5D_2$, $^5D_1$ and $^5D_0$ levels, indicated by arrows 7. As mentioned above, the decay times of transitions from ^5D_J levels with $J > 0$ are about 10 times shorter than these from $^5D_0$,[33] which enhances efficient energy transfer and hence rather fast quenching of the Y_2O_3 emission upon increasing the Eu^{3+} concentration.[2,35] In terms of the probability S in eqn (3) it means that energy from an e–h pair is transferred to a Eu^{3+} ion.

At low Eu^{3+} concentrations <2 mol% the strong intrinsic emission at 28 300 cm^{-1} may be absorbed by Eu^{3+} ions in the lattice: this process is indicated by arrows (5) and (6) in Fig. 10. It has been indicated in this figure that the Y_2O_3 UV radiation is

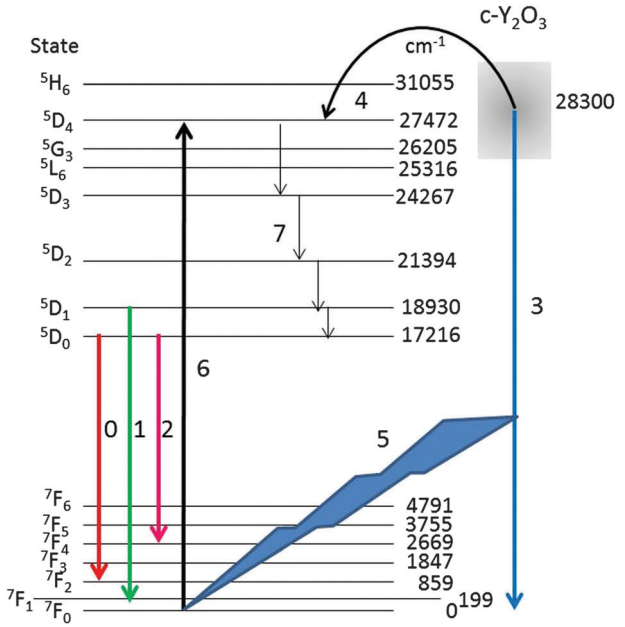

Fig. 10 Energy levels of Eu^{3+} in Y_2O_3. The broad intrinsic luminescence of Y_2O_3 has been represented at 28 300 cm^{-1} by arrow (3). The arrows (0), (1) and (2) refer to the $^5D_0 \rightarrow {}^7F_2$, $^5D_1 \rightarrow {}^7F_1$ and $^5D_0 \rightarrow {}^7F_4$ Eu^{3+} transitions respectively, while (4) indicates the radiationless energy transfer from Y_2O_3 to Eu^{3+}. For arrows (5), (6) and (7) we refer to text.

absorbed from the ground level $^7F_0$; hence, the $^5D_4$ Eu^{3+} level will be populated more densely. As mentioned above, from $^5D_4$ energy will trickle down to the lower ^5D_J levels. The process indicated by arrows (5) and (6) will stop when the intrinsic luminescence of Y_2O_3 has quenched at large Eu^{3+} concentration. The latter process explains the high value of R_1 in Fig. 9 and similarly the rather strong $^5D_1 \rightarrow {}^7F_J$ and $^5D_2 \rightarrow {}^7F_J$ transitions in Fig. 4B–D. The foregoing consideration also explains why the ratio R_1 in Fig. 9 at low temperature is higher than at room temperature: the process indicated by the arrows (5) and (6) is more dominant at low temperature because of the much stronger UV luminescence of Y_2O_3.

4. Conclusions

In the preceding sections we have described the cathodoluminescence of undoped Y_2O_3 and Y_2O_3:Eu^{3+} crystals in the TEM by high-energy electron bombardment. At low temperatures we observed a broad emission band at about 353 nm, which has been ascribed to the migration of excitons to luminescence centres in Y_2O_3. We found that the UV/blue luminescence is strongly temperature dependent and that at concentrations >2 mol% Eu^{3+} no blue light could be detected.

The temperature behaviour of the intrinsic luminescence of Y_2O_3 has been explained with a model for the self-trapped excitons. The depth of these traps was found to be 0.14 eV. The concentration dependence of the UV/blue luminescence has been explained by the good overlap between the level of the blue Y_2O_3 band and the $^5D_4$ level of the Eu^{3+} ion. The strong radiance of $^5D_1 \rightarrow {}^7F_J$ and $^5D_2 \rightarrow {}^7F_J$ Eu^{3+} transitions in the spectra excited at 200 keV in Y_2O_3:Eu^{3+} with low Eu^{3+} concentration has been explained by absorption of the intrinsic Y_2O_3 radiation by Eu^{3+} ions. Although we have presented a detailed explanation of the concentration and temperature behaviour of the UV/blue emission, we have also generated new questions. The most important is about the nature of the red emission bands at 675 nm and 770 nm.

Based on the results described in this article we would like to make a suggestion to other scientists working with electron microscopes in the field of biomedical imaging with phosphors. This fast growing technology has recently been reviewed by Gai *et al.*[36] Since undoped Y_2O_3 or Y_2O_3:Eu^{3+} with low Eu^{3+} concentration will manifest the strong intrinsic luminescence of Y_2O_3 in the e-beam of a TEM (and likely also in a SEM) at low temperatures, we think that this work opens new perspectives for labelling (biological) samples with nanocrystals of Y_2O_3:Eu^{3+}.

Acknowledgements

We are grateful to the EPSRC and the Technology Strategy Board (TSB) for funding the PURPOSE (TP11/MFE/6/I/AA129F; EPSRC TS/G000271/1), CONVERTED (JeS no. TS/1003053/1) and PRISM (EP/N508974/1) programs. We are also grateful to the TSB for funding the CONVERT program.

References

1 *Phosphor Handbook*, ed. W. Yen, S. Shionoya and H. Yamamoto, CRC Press, Boca Raton, 2nd edn, 2007.
2 G. Blasse and B. C. Grabmaier, *Luminescent Materials*, Springer-Verlag, Berlin, 1994.
3 L. Ozawa, *Cathodoluminescence, Theory and Applications*, Kodansha & VCH, Verlag, Tokyo, 1990.
4 G. Li and J. Lin, *Chem. Soc. Rev.*, 2014, **43**, 7099.
5 D. den Engelsen, P. G. Harris, T. G. Ireland and J. Silver, *ECS J. Solid State Sci. Technol.*, 2014, **3**, R53.
6 K. A. Wickersheim and R. A. Lefever, *J. Electrochem. Soc.*, 1964, **111**, 47.
7 A. Fukabori, L. An, A. Ito, V. Chani, K. Kamada, A. Yoshikawa, T. Ikegami and T. Goto, *Ceram. Int.*, 2012, **38**, 2119.
8 A. Konrad, U. Herr, R. Tidecks, F. Kummer and K. Samwer, *J. Appl. Phys.*, 2001, **90**, 3516.
9 L. G. Jacobsohn, B. L. Bennett, R. E. Muenchausen, J. F. Smith and D. W. Cooke, *Proc. SPIE*, 2006, **6321**, 63210J.
10 R. L. Wood and W. Hayes, *J. Phys. C: Solid State Phys.*, 1982, **15**, 7209.
11 T. C. de Oliveira, M. Souza da Silva, L. Menezes de Jesus, D. Vieira Sampaio, J. C. Alves dos Santos, N. R. da Silva Souza and R. Santos da Silva, *Ceram. Int.*, 2014, **40**, 16209.
12 P. A. Tanner, L. Fu and B. M. Cheng, *J. Phys. Chem. C*, 2009, **113**, 10773.
13 G. Blasse and L. H. Brixner, *Eur. J. Solid State Inorg. Chem.*, 1991, **28**, 767.

14 W. Hayes, M. J. Kane, O. Salminen and A. I. Kuznetsov, *J. Phys. C: Solid State Phys.*, 1984, **17**, L383.
15 A. Fukabori, V. Chani, J. Pejchal, K. Kamada, A. Yoshikawa and T. Ikega, *Opt. Mater.*, 2011, **34**, 452.
16 Y. Fujimoto, T. Yanagida, Y. Yokota, A. Ikesue and A. Yoshikawa, *Opt. Mater.*, 2011, **34**, 448.
17 C. D. Cress, C. S. Redino, B. J. Landi and R. P. Raffaelle, *J. Solid State Chem.*, 2008, **181**, 2041.
18 Y. Ato, R. Huzimura and L. Ozawa, *Jpn. J. Appl. Phys.*, 1968, **7**, 1497.
19 L. Ozawa, *Appl. Phys. Lett.*, 1977, **31**, 694.
20 W. Hayes, *J. Lumin.*, 1984, **31**, 99.
21 A. Lushchik, M. Kirm, Ch. Lushchik, I. Martinson and G. Zimmerer, *J. Lumin.*, 2000, **87–89**, 232.
22 D. B. Williams and C. B. Carter, *Transmission Electron Microscopy, A Textbook for Materials Science*, Springer, New York, 2009.
23 D. den Engelsen, P. G. Harris, T. G. Ireland and J. Silver, *ECS J. Solid State Sci. Technol.*, 2015, **4**, R1.
24 D. den Engelsen, P. G. Harris, T. G. Ireland, R. Withnall and J. Silver, *ECS J. Solid State Sci. Technol.*, 2013, **2**, R201.
25 X. Jing, T. Ireland, C. Gibbons, D. J. Barber, J. Silver, A. Vecht, G. Fern, P. Trogwa and D. C. Morton, *J. Electrochem. Soc.*, 1999, **146**, 4654.
26 J. Silver, T. G. Ireland and R. Withnall, *J. Electrochem. Soc.*, 2004, **151**, H66.
27 G. R. Fern, A. Lipman, J. Silver, A. Howkins, T. G. Ireland, P. Marsh, D. den Engelsen, *Proceedings of 22nd International Display Workshops*, December 9–11, Otsu, Japan, 2015.
28 J. V. Jelley, *Čerenkov Radiation and its applications*, Pergamon Press, London, 1958.
29 Y. Nigara, *Jpn. J. Appl. Phys.*, 1968, **7**, 404.
30 D. den Engelsen, P. G. Harris, T. G. Ireland and J. Silver, *ECS J. Solid State Sci. Technol.*, 2015, **4**, R1.
31 V. B. Mikhailik and H. Kraus, *Phys. Status Solidi B*, 2010, **247**, 1583.
32 G. Blasse, *J. Lumin.*, 1994, **60–61**, 930.
33 D. B. M. Klaasen, R. A. M. van Ham and T. G. M. van Rijn, *J. Lumin.*, 1989, **43**, 261.
34 J. Wen, L. Hu, M. Yin and S. Xia, *Current Appl. Phys.*, 2012, **12**, 732.
35 D. L. Dexter, *J. Chem. Phys.*, 1953, **21**, 836.
36 S. Gai, C. Li, P. Yang and J. Lin, *Chem. Rev.*, 2014, **114**, 2342.

